Obesity resistance and deregulation of lipogenesis in Δ6-fatty acid desaturase (FADS2) deficiency

Wilhelm Stoffel[1,2,*], Ina Hammels[1,2], Britta Jenke[1,2], Erika Binczek[1], Inga Schmidt-Soltau[1], Susanne Brodesser[2], Margarete Odenthal[3] & Mario Thevis[4]

Abstract

Δ-6-fatty acid desaturase (FADS2) is the key enzyme in the biosynthesis of polyunsaturated fatty acids (PUFAs), the essential structural determinants of mammalian membrane lipid-bilayers. We developed the auxotrophic *fads2*$^{-/-}$ mouse mutant to assess the enigmatic role of ω3- and ω6-PUFAs in lipid homeostasis, membrane structure and function. Obesity resistance is another major phenotype of the *fads2*$^{-/-}$ mutant, the molecular basis of which is unknown. Phospholipidomic profiling of membrane systems of *fads2*$^{-/-}$ mice revealed diacylglycerol-structures, deprived of PUFAs but substituted with surrogate eicosa-5,11,14-trienoic acid. ω6-Arachidonic (AA) and ω3-docosahexaenoic acid (DHA) supplemented diets transformed *fads2*$^{-/-}$ into *AA-fads2*$^{-/-}$ and *DHA-fads2*$^{-/-}$ mutants. Severely altered phospholipid-bilayer structures of subcellular membranes of *fads2*$^{-/-}$ liver specifically interfered with maturation of transcription factor sterol-regulatory-element-binding protein, the key regulator of lipogenesis and lipid homeostasis. This study strengthens the concept that specific PUFA-substituted membrane phospholipid species are critical constituents of the structural platform operative in lipid homeostasis in normal and disease conditions.

Introduction

The role of ω3- and ω6- PUFAs in lipid homeostasis and related imbalances in several pathologies have been the subject of intense research for several decades [1]. Evidence accumulating during the last decades suggests that the genetic basis of lipid homeostasis is critically regulated by epigenetic factors, particularly nutritional imbalances. The ω3/ω6-PUFA ratio in the Western diet is regarded as the driving force in the development of chronic metabolic, vascular [2–5], psychiatric and neurodegenerative disorders [6].

Dietary studies have been the approach to better define the systemic role of ω3- and ω6-PUFAs in lipid homeostasis and the molecular pathogenesis of these diseases. Subsequently, a broad range of therapeutic implementations have been proposed. However, until the precise roles of ω3- and ω6-PUFAs are better understood, treatment of PUFA-related diseases may not be adequate.

Mammalian cells transform essential fatty acids (EFAs) ω3-α-linolenic (α-18:3; ALA) and ω6-linoleic (18:2; LA) acid at fatty acid desaturase- and elongase- complexes, localized in the endoplasmic reticulum (ER), into long-chain ω3- and ω6-PUFA families, that include ω3-eicosapentaenoic (20:5^{5,8,11,14,17}, EPA), ω3-docosahexaenoic acid(22:6^{4,7,10,13,16,19}, DHA), ω6-di-homo-γ-linolenic (20:3^{8,11,14}), and ω6-arachidonic acid (20:4^{5,8,11,14}, AA). PUFAs are incorporated into the diacylglycerol (DAG)-backbone of respective phospholipids (PLs) by specific acyl-transferases during *de novo* synthesis [7] or by the deacylation-reacylation cycle [8]. PLs are amphipathic molecules with 'dove tail' functions, asymmetrically distributed in the outer leaflet [phosphatidyl-choline (PC) and sphingomyelin (SM)] and inner leaflet [phosphatidyl -ethanolamine, PE, -inositol, PI, -serine, PS and bis-phosphatidyl-glycerol, CL (cardiolipin)]. PUFAs are structural determinants within the hydrophobic DAG-core, where they contribute to the hydrophobic scaffold of functionally divergent integral membrane proteins. Their polar head groups at the membrane surface function as docking sites of protein domains in cellular transport and cell signaling.

We applied the loss of structure-function strategy to studies *in vivo* on the molecular mechanism(s) underlying the structural and metabolic role of individual PUFAs. This approach has become feasible in the *fads2*$^{-/-}$ mouse mutant [9]. Systemic absence of PUFAs and auxotrophy of the *fads2*$^{-/-}$ mouse mutant are essential prerequisites for conclusive dietary studies *in vivo*.

Infertility of male and female *fads2*$^{-/-}$ mice was the first dominant phenotype analyzed [9]. The rescue of male and female fertility by a 22:6- (DHA) supplemented diet gave the first hint at the

auxotrophy of the $fads2^{-/-}$ mutant. Incorporation of specifically DHA into PLs of Sertoli and follicular granulosa cells rescued cell polarity, germ cell maturation and fertility. These results have been confirmed in another $fads2^{-/-}$ mouse model [10,11].

We report here on another major phenotype of the $fads2^{-/-}$ mutant, perturbed lipogenesis and obesity resistance, and the molecular link to PUFA deficiency.

Profiling of the membrane phospholipidomes of the metabolically most active tissues, liver, muscle, brown adipose tissue (BAT) and white adipose tissue (WAT) generated the structural platform for the phenotypic characterization.

The first striking observation was the activation of a novel abnormal pathway, by which LA acid was transformed into the eicosatrienoic acid ω6-20:3[5,11,14] with a non canonical double-bond system. Second, 20:3[5,11,14] was systemically incorporated as a surrogate of PUFAs, specifically of AA (ω6-20:4[5,8,11,14]), into DAGs of all membrane PLs. Third, the severely perturbed core structures of subcellular membranes (ER-, Golgi- and nuclear) critically altered the hydrophobic environment for functions of integral membrane proteins, specifically of ER/Golgi membrane-bound posttranslational processing of SREBP1c, a key transcription factor in the regulation of lipid metabolism. Fourth, this altered the expression of key enzymes of lipogenesis in the $fads2^{-/-}$ mouse.

Finally, we observed that stringent dietary supply of AA systemically transformed the auxotrophic nd-$fads2^{-/-}$ mutant into the 'ω6-$AA^{-/-}$' and DHA into the 'ω3-$DHA^{-/-}$' mouse line with solely AA and DHA, respectively. These three well defined mouse lines of $fads2^{-/-}$ expand the scope of studies, which target the numerous proposed but experimentally unproven functions of PUFAs in normal and disease conditions.

Results and Discussion

Fads2$^{-/-}$ mice show obesity resistance

FADS2-deficient mice are obesity-resistant. Adult male and female nd-$fads2^{-/-}$ mice are lean and 10–15% smaller in body size than $nd^{+/+}$ mice (Fig 1A and B). Weight gain of $fads2^{-/-}$ littermates slowed down after weaning and differed from $fads2^{+/+}$ by 20 and 25% at age 4–5 months. $AA^{+/+}$ and $^{-/-}$ mice gained weight at a

similar but enhanced rate, but less than nd-$fads2^{+/+}$ and $^{-/-}$ mice on DHA supplemented diet (Fig 1C). Non-invasive NMR revealed a reduction of body fat mass by 10% and correspondingly an increase in lean mass of body weight of $fads2^{-/-}$ mice (Fig 1D and E). Weight differences of liver, BAT, and WAT of nd-, AA- and $DHA^{+/+}$ and $^{-/-}$ mice are depicted in Fig 1F. Mass of subcutaneous, abdominal and epididymal adipose tissues of nd- and $AA^{-/-}$ mice remained markedly reduced during life span, but mass of WAT of adult (4 months) $DHA^{-/-}$ mice was twice that of $DHA^{+/+}$ mice. Size of adipocytes were estimated from area measurements in sections of epididymal WAT.

Adipocytes of $nd^{-/-}$ mice were about two-third in size of $nd^{+/+}$ mice, about one third in $AA^{-/-}$ and half in $DHA^{-/-}$ mice (Fig 1G and H). Situs of age- and gender-matched nd-, AA- and $DHA^{+/+}$ and $^{-/-}$ littermates underlined these parameters (supplementary Fig S1A–F).

The loss of adipose tissue of $nd^{-/-}$ mice was associated with reduced levels of serum leptin, 1.8 ± 0.43 ng/ml in $nd^{+/+}$ to 0.8 ± 0.4 ng/ml in $nd^{-/-}$ mice. Leptin levels were similar in $AA^{+/+}$ and $AA^{-/-}$ mice, 1.25 ± 0.4 and 1.2 ± 0.3 ng/ml, respectively, and those of $DHA^{+/+}$ mice were elevated (6 ± 2 ng/ml), but normal in $DHA^{-/-}$ mice (1.2 ± 0.4 ng/ml) ($n = 10$). nd $fads2^{-/-}$ mice showed significantly reduced serum triglyceride and cholesterol concentrations (supplementary Fig S1G and H).

Leanness of nd-$fads2^{-/-}$ was not caused by reduced food uptake, malabsorption or maldigestion. Phenomaster recordings documented a similar food uptake of nd- and $AA^{+/+}$ and $^{-/-}$ mice (supplementary Fig S1I). $DHA^{+/+}$ and $DHA^{-/-}$ mice, however, were hyperphagic (supplementary Fig S1J). Metabolic parameters (VO$_2$ uptake, VCO$_2$ production, and heat dissipation) of $nd^{-/-}$ mice were reduced by approximately one third compared to control mice (supplementary Fig S2C–E), but comparable and unchanged in AA- or $DHA^{+/+}$ and $^{-/-}$ mice. RER reflected a balanced carbohydrate and fat utilization by the three cohorts (supplementary Fig S2).

Enhanced energy production due to perturbed epidermal lipid barrier with trans-epidermal water loss (TEWL) and associated metabolic waste syndrome were excluded by measurement of TEWL of the nd-$fads2^{-/-}$ mutant (supplementary Fig S2A).

Locomotor activity of adult (3–5 months) nd-, AA- and $DHA^{+/+}$ and $^{-/-}$ mice was compared in the Phenomaster (supplementary Fig S2B). Locomotor activity of nd- and $DHA^{-/-}$ mice was reduced

---

Figure 1. *Fads2$^{-/-}$* mice develop obesity resistance.

A–C   Body size [cm] (nose-tail root) and weight of male and female $fads2^{-/-}$ mice (age 4 months) differed by about 20 and 25% from control $^{+/+}$ mice (A, B), similarly of female $DHA^{-/-}$, unlike those of $AA^{-/-}$ ($n = 20$) (C).

D, E   NMR-spectroscopy revealed significantly reduced% fat mass (D) and correspondently elevated% lean mass of body weight in $fads2^{-/-}$ ($n = 10$) (E).

F   Wet weight [g] of WAT of $fads2^{+/+}$ and $AA^{+/+}$ (black bars) was four and three times and of BAT about twice higher than that of corresponding $fads2^{-/-}$ mice. Weight of WAT and BAT of $DHA^{-/-}$ exceeded twice that of $DHA^{+/+}$ mice ($n = 10$). Liver weight of nd-, AA- and $DHA^{+/+}$ mice was 1.3, 1.5 and 1.2 times higher than that of corresponding $fads2^{-/-}$ mice.

G, H   In HE-stained sections (5 μm) epididymal adipocytes of $nd^{+/+}$ were significantly larger than epididymal adipocytes of $nd^{-/-}$ mice, about three times in AA- and twice in $DHA^{+/+}$ mice.

I   Glucose tolerance test (GTT) (15 min $P = 0.0342$, 30 min $P = 0.0019$, 60 min $P = 0.0130$, 120 min $P = 0.0271$) of nd-$fads2^{+/+}$ and $^{-/-}$ mice (red).

J   Insulin tolerance test (ITT) (15 min $P = 0.030$, 30 min $P = 0.0001$, 60 min $P = 0.0005$, 120 min $P = 0.030$) of nd-$fads2^{+/+}$ and $^{-/-}$ mice (red).

K   Normal GTT of $AA^{+/+}$ and $AA^{-/-}$ mice ($n = 10$).

L   Normal ITT of $AA^{+/+}$ and $AA^{-/-}$ mice ($n = 10$).

M   GTT of $DHA^{+/+}$ and $DHA^{-/-}$ mice ($n = 10$).

N   ITT of $DHA^{+/+}$ and $DHA^{-/-}$ mice ($n = 10$).
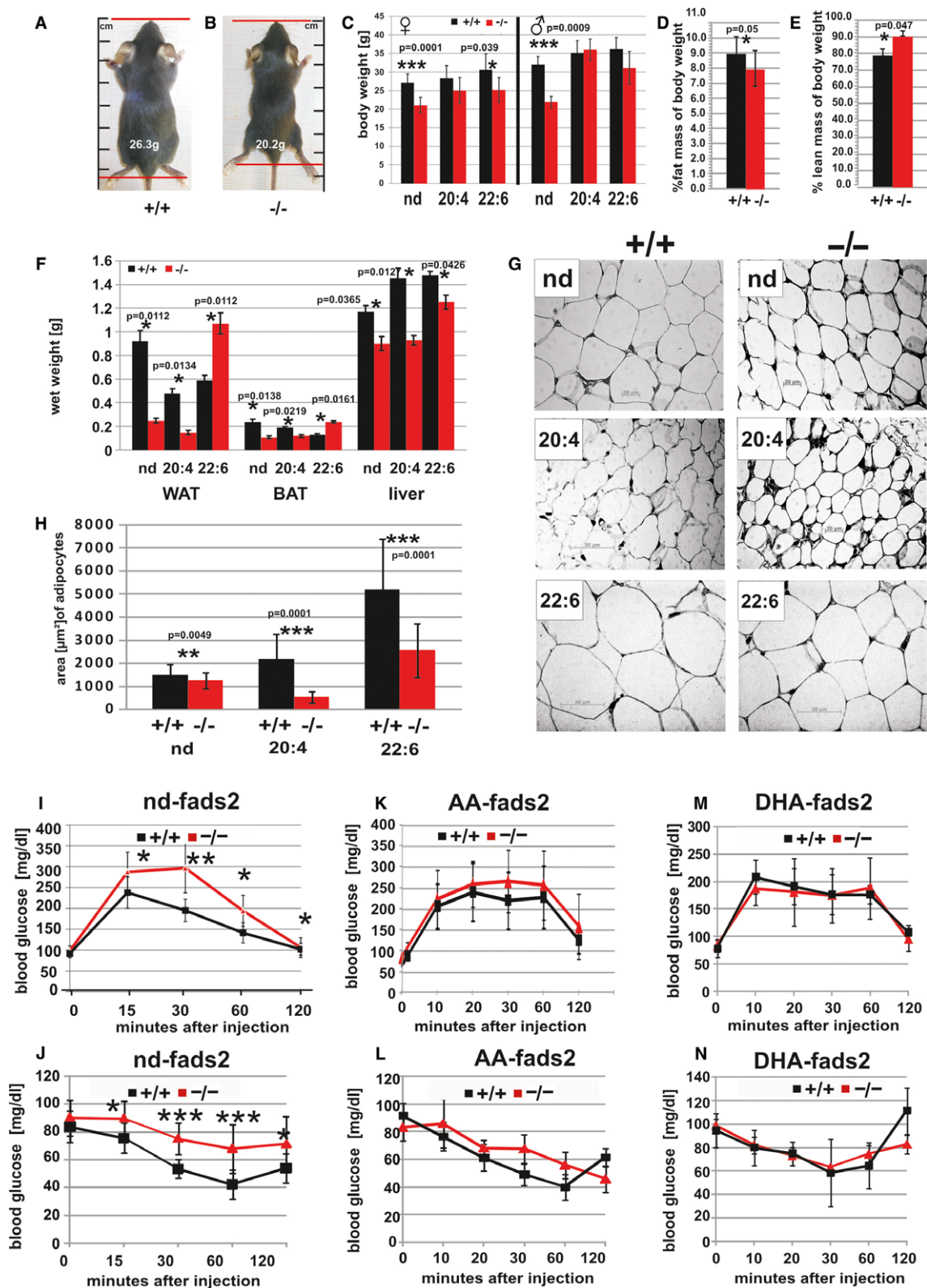
to one third due to the absence of the two main anandamides (*N*-arachidonoyl-ethanolamine and 2-arachidonoyl-glycerol) in brain extracts of respective cohorts of $nd^{-/-}$ and $DHA^{-/-}$ mice, but $AA^{-/-}$ mice showed normal motility (data not shown). We next searched for biochemical and cellular links between altered lipid metabolism and strongly reduced adipogenesis in the $fads2^{-/-}$ mouse.

Insulin response in the $fads2^{-/-}$ mouse is altered

Fasting serum insulin concentration of $fads2^{-/-}$ mice is about half that of $^{+/+}$ littermates, whereas in *AA*- and $DHA^{-/-}$ mice have normal serum insulin concentrations. The glucose tolerance test (GTT) of $nd^{+/+}$ and $^{-/-}$ mice (Fig 1I) showed a significantly retarded return to normal serum glucose concentration in the $nd^{-/-}$ mouse during the 2 h period post intraperitoneal insulin application, suggesting reduced insulin sensitivity, which is also reflected in the insulin tolerance test (ITT) (Fig 1J). GTTs and ITTs of *AA*- and $DHA^{+/+}$ and $^{-/-}$ mice showed a similar responses (Fig 1K–N).

Severe perturbationof the nd-$fads2^{-/-}$ membrane phospholipidome

PUFAs are ubiquitous substituents of the DAG moiety of all PL classes of mammalian tissues. To unravel the mechanisms that link PUFA deficiency and deregulated lipogenesis in the $nd^{-/-}$ mouse, we defined the structural platform by a comprehensive analysis of the phospolipidome of the four metabolically most active tissues liver, muscle, BAT and WAT. PL classes were separated by high-performance thin-layer chromatography (HPTLC) for MS/MS using precursor scanning characteristic for each PL class, depicted for $fads2^{+/+}$ and $^{-/-}$ liver. The flow diagram in supplementary Fig S3A paradigmatically outlines the separation, isolation, and characterization of individual species of PI of total lipid extract of liver of $fads2^{+/+}$ and $^{-/-}$ mice by MS/MS. Further detailed structural insight into DAG species of each PL class was obtained by GC/MS analysis of their FA substituents as methylesters.

The first surprising discovery was the induction of a futile biosynthetic pathway, by which LA was transformed into a novel non-mammalian *all-cis*-eicosa-5,11,14-trienoic acid ($20:3^{5,11,14}$) for substitution of PL-associated DAGs in the $fads2^{-/-}$mouse (Fig 2A and B). $20:3^{5,11,14}$ was systemically incorporated as a surrogate of AA and PUFAs in the main PL classes PC, PI, PS and PE, not in cardiolipin (Fig 2C and D).

The structure of this unusual PL constituent was established unambiguously by GC/MS analysis of its DMOX (2,2-dimethyl oxazoline) derivative. DMOX derivatives of PUFAs release diagnostic fragments in MS, characteristic of the methylen-interrupted double-bond systems [12–15].The analytical data were identical with those of synthetic DMOX-$20:3^{5,11,14}$ [16] and spectra from published data [13] (Fig 2E and F). The double-bond positions of $20:3^{5,11,14}$ were confirmed finally by oxidative ozonolysis, which released the expected adipic and glutaric acids, identified as dimethylesters by GC/MS, (supplementary Fig S3).

The analytical data suggested the activation of a novel futile pathway from LA via chain elongation to $20:2^{11,14}$ and $\Delta5$-desaturation to $20:3^{5,11,14}$ in the $nd^{-/-}$ mouse.

We next studied the distribution of $20:3^{5,11,14}$ in DAGs of PC, PI, PS, and PE in the phospholipidome of liver total lipid extract of nd-$fads2^{-/-}$ mice and their microsomal and nuclear membrane fractions, muscle, BAT, and WAT (supplementary Fig S4), the meta-bolically most active tissues in the $nd^{-/-}$ mouse. Stoichiometry and distribution of $20:3^{5,11,14}$ in different PL classes in $nd^{-/-}$ mice were close to that of respective $20:4^{5,8,11,14}$ in $fads2^{+/+}$mice (Fig S3). No $\Delta5$-desaturation of $18:2^{9,12}$ to $18:3^{5,9,12}$ or α-$18:3^{9,12,15}$ to $18:4^{5,9,12,15}$ was observed. These findings underline the high chain-length specificity of $\Delta5$-desaturase (FADS1).

Transforming the nd-$fads2^{-/-}$ into the 'arachidonic acid (AA)-' and 'docosahexaenoic acid (DHA)-$fads2^{-/-}$' mouse mutants

We asked whether $20:3^{5,11,14}$ substituted PLs in mammalian membrane systems can match the structural and functional properties of AA and DHA. Unexpectedly, $nd^{-/-}$ mice, when raised on 20:4- (AA) and 22:6- (DHA) supplemented diets, completely suppressed the synthesis of $20:3^{5,11,14}$. $20:3^{5,11,14}$ was systemically replaced by 20:4 and 22:6 in respective PL classes of *AA*- and $DHA^{-/-}$ mice, as depicted for total liver and its purified nuclear and ER- membranes, and of muscle, BAT, and WAT (supplementary Fig S4).

These *in vivo* studies were confirmed by experiments in primary hepatocyte cultures from $nd^{+/+}$ and auxotrophic $nd^{-/-}$ mice. Supplementary Fig S5 depicts the utilization of $20:4^{5,8,11,14}$ (AA) and $\omega6$-$20:3^{5,11,14}$ in the synthesis of PL classes in $^{+/+}$ and $^{-/-}$ primary hepatocytes. sn2-O-Acyltransferases of the family of membrane-bound O-acyltransferases (MBOAT) [17] showed no preference for either substrate in *de novo* synthesis or PL remodelling.

In conclusion, these dietary studies generated three well-defined $fads2^{-/-}$ mouse models: (i) the $nd^{-/-}$ mouse, all PL classes of which lack the canonical $\omega3$- and $\omega6$-PUFAs but instead are acylated exclusively with $20:3^{5,11,14}$ as PUFA surrogate, (ii) the '$\omega6$-*AA*-$fads2^{-/-}$' mouse with $\omega6$-arachidonic acid, and (iii) the '$\omega3$-*DHA*-$fads2^{-/-}$' mouse with $\omega3$-docosahexaenoic acid as the only PUFA as substituent in the sn2-position of DAGs of membrane PLs in the membrane lipid bilayer. The $AA^{-/-}$ mouse resembles a mimicry of mammalian solely on the 'land food web' and the $DHA^{-/-}$ of the 'sea food chain' during evolution [1].

Gene expression of enzymes of lipid metabolism in $fads2^{-/-}$ mice

We next investigated the expression profiles of genes coding for transcription factors of enzymes involved in lipid metabolism *pparα, ß, γ, srebp1c, hmgcoas2, hnf1α, hnf4α* and enzymes of fatty acid metabolism *cpt1* and *2, scd1-3, $\Delta5$ (fads1)* and *elongases 2–6* and of gluconeogenesis *fruct-1,6-bp, glc-6p* and *pepck* of (i) the nd-*fads2* (Fig 5A and B), (ii) the *AA*- (Fig 5C and D) and (iii) the $DHA^{+/+}$ and $^{-/-}$ mice (Fig 5E and F) by real time qRT-PCR. (i) Gene expression of enzymes involved in gluconeogenesis did not change significantly in $nd^{+/+}$ and $^{-/-}$ liver, except for the upregulation of *glc-6p* in $DHA^{-/-}$ mouse liver (Fig 5A and B). Also expression of transcription factors of lipogenesis, including *pparα, ß, γ, hnf1α and hnf4α*, and *srebp1c*, and enzymes of cholesterol synthesis (*HMGCoA synthase*) were not significantly changed in $nd^{-/-}$ liver. However, steady-state concentrations of the RNA of key enzymes of PUFA synthesis, the SCD1-3 and desaturase $\Delta5$ (FADS1) subunit of the trimeric microsomal desaturase complexes, and the condensing subunits of the tetrameric elongase complexes ELOVL2, 5 and 6 were remarkably elevated. ELOVL2 in *nd*-, *AA*- and $DHA^{-/-}$ liver is essential for the synthesis of $\omega6$-very long chain PUFAs (VLCFA) [18]. 18:2 and γ-18:3 are the preferred substrates of ELOVL5 [19]. *Elovl3* expression was downregulated and thereby the synthesis of saturated VLCFA and recruitment of saturated triglycerides to BAT [20], but *elovl6*,
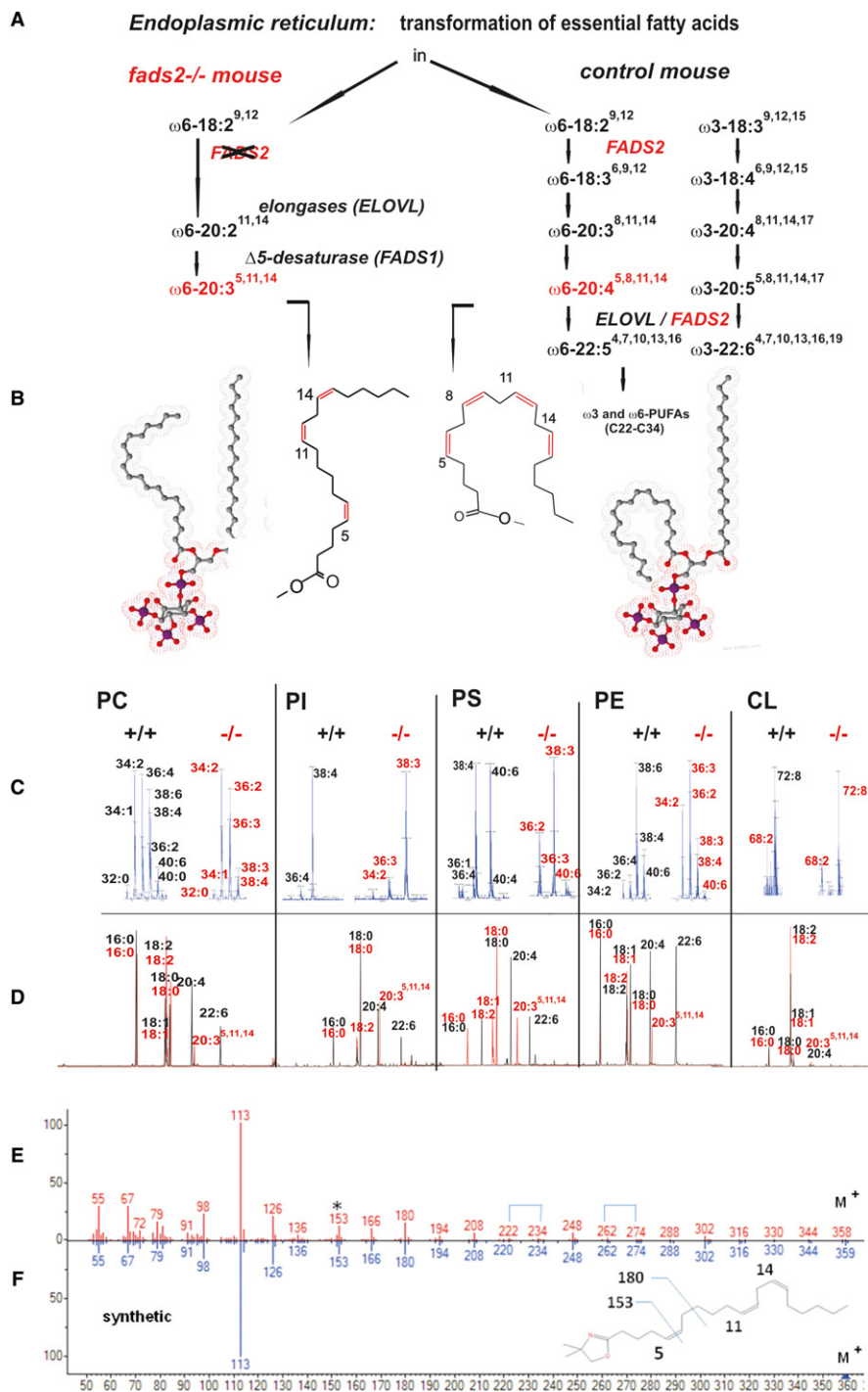
Figure 2. Linoleic acid is transformed in a non-canonical reaction sequence to the non-mammalian 'FADS2-deficiency' eicosa-5z,11z,14z-trienoic acid (20:3[5,11,14]).

A   Pathway of the transformation of linoleic acid, canonical (right) and aberrant to 20:3[5,11,14] (left) in the *fads2*^{−/−} mouse.

B   Space filling models of 18:0/20:4[5,8,11,14]-PIP3 and 18:0/20:3[5,11,14]-PIP3.

C   MS/MS of PC, PI, PS, PE, and cardiolipin species of total lipid extract. Numbers at peaks represent the sum of C-atoms and number of double bonds in acyl-chains of DAGs in respective PL species.

D   GC/MS of FAME of substituents of DAGs of individual PL species. Black bars, [+/+]; red bars, [−/−].

E, F   Structural characterization (head-to-tail presentation) by GC/MS of 2,2-dimethyloxazoline (DMOX) derivatives of 20:3[5,11,14], of unknown C20-PUFA of liver PI as 20:3[5,11,14] (E) and of synthetic 20:3[5,11,14](F).
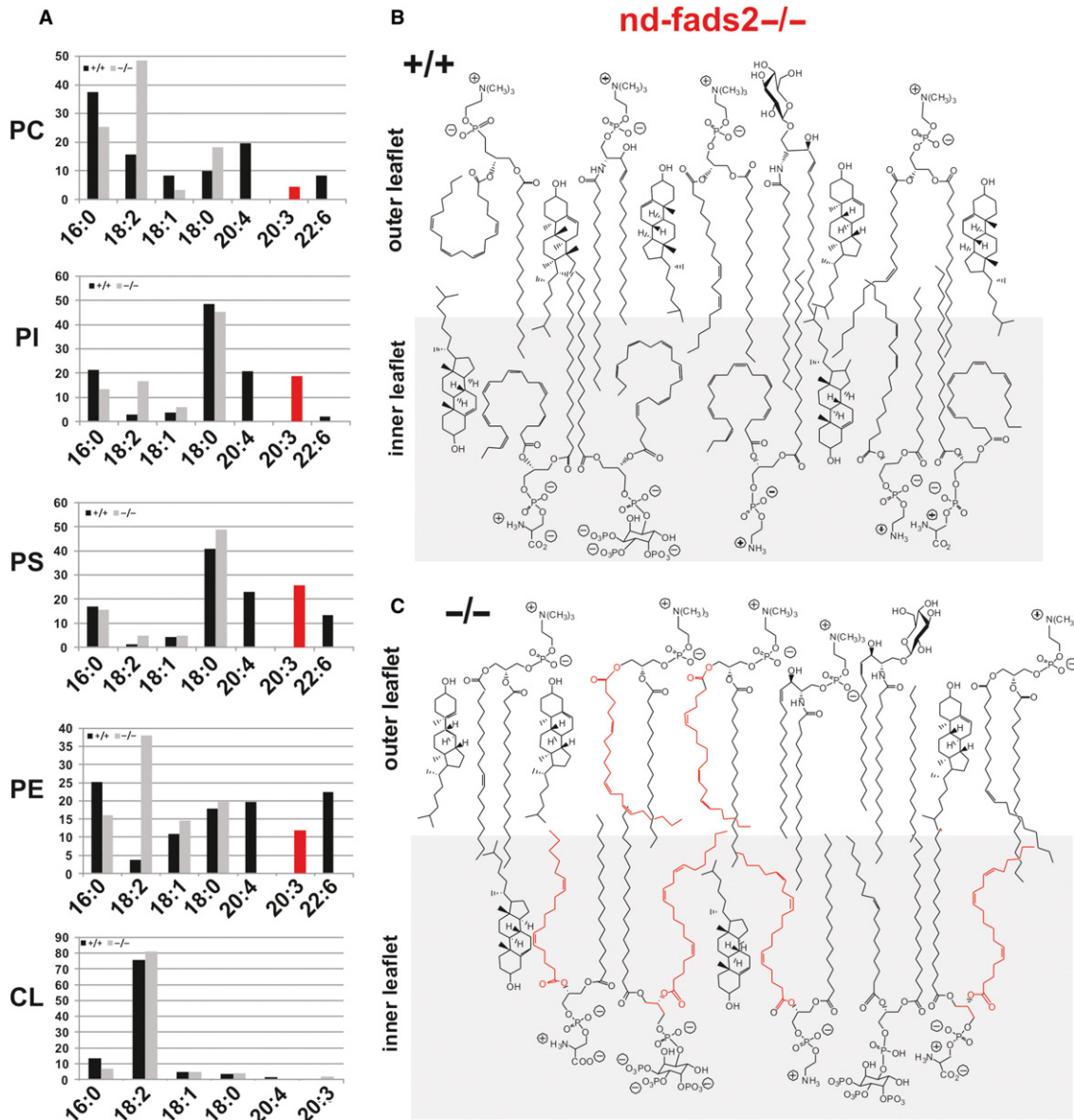
Figure 3. Phospholipidome of total liver unveils the absence of all PUFAs and their substitution by surrogate 20:3^{5,11,14}.

A   Profiling of the phospholipidome of total liver of *fads2*$^{+/+}$ (black) and $^{-/-}$ (red) mice (age 4 months). GC/MS of FAME of substituents of DAGs of individual PC, PI, PS, PE, and cardiolipin species. Black bars, $^{+/+}$; grey bars, $^{-/-}$. Aberrant 20:3^{5,11,14} (red bar) is the only PUFA in PLs of liver. *y*-axis,% of total FAME.

B, C   Schematic presentation of the assembly of PL species in a domain of the asymmetric bilayer of membranes of control $^{+/+}$ (B) and *fads2*$^{-/-}$ mice (C), and highlights the severely distorted inner leaflet of the bilayer.

which encodes the elongase of saturated C12–C16 fatty acids and also correlates positively with the severity of hepatosteatosis was overexpressed. These enzymes are major targets of SREBP1c, critically involved in the development of obesity and insulin resistance. (ii) In $AA^{-/-}$ liver only the expression of *ppar*γ, the transcription factor of key enzymes of lipid metabolism, and of *elovl2* was significantly upregulated (Fig 5C and D). (iii) $DHA^{-/-}$ mouse liver showed elevated expression of *glc-6p* indicating enhanced gluconeogenesis, and of transcription factor *srebp1c* causing the activation of

Δ5 desaturases *(fads1)* and *elovl2* and *elovl5* and of *elovl1*, the elongase yielding 24:0 to 26:0, required for ceramide synthesis. Expression of *scd3*, a mouse-specific isoform of stearoyl-CoA desaturase, was down regulated in $DHA^{-/-}$ mice (Fig 5E and F).

Deregulation of lipogenesis and hepatic steatosis in the *fads2*$^{-/-}$ mouse

Lipid homeostasis and lipid bilayer structures of the ER and Golgi membranes are stringently controlled by SREBP1c, the key
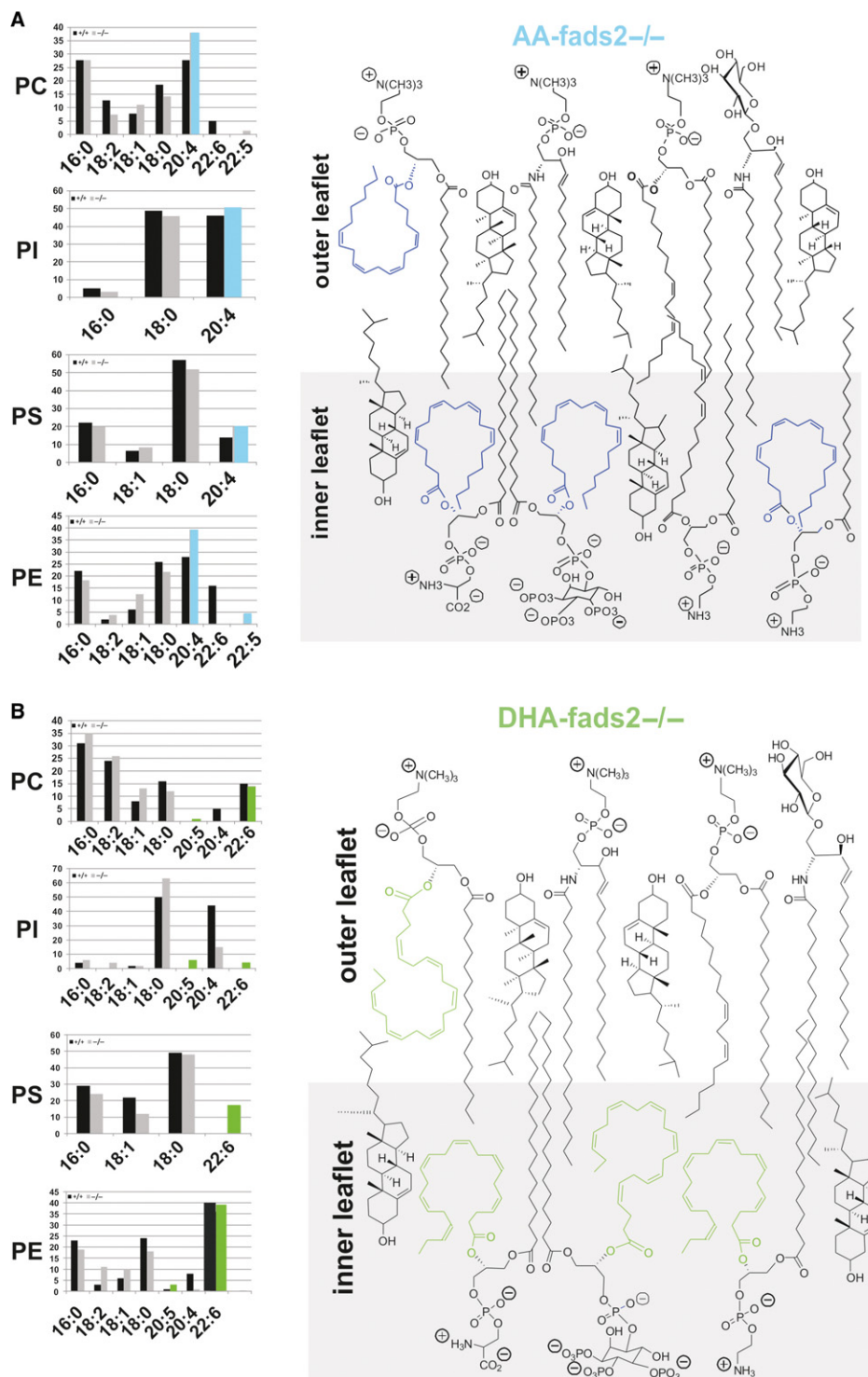
Figure 4. Dietary arachidonic (AA) and docosahexaenoic (DHA) acid transform the auxotrophic *nd-fads2*^{−/−} mouse into the 'AA-' and 'DHA-fads2*^{−/−}' mouse mutants.

A   AA and DHA supplemented diets systemically suppress the synthesis of 20:3[5,11,14]. The bar diagrams present the quantitative analysis of the fatty acid substituents of the main PL classes of liver of AA^{−/−} mice. AA (blue) are the only surrogates for PUFAs in all PL species. y-axis:% of total FAME. Right panel: schematic structural view of the putative assembly of AA-substituted PL classes enriched in the inner leaflet of the PL bilayer in a domain of the asymmetric membrane bilayer.

B   Same as in (A) for DHA^{−/−} mice. DHA (green) are the only surrogates for PUFAs in all PL species. y-axis:% of total FAME. Right panel: schematic structural view of the putative assembly of DHA-substituted PL classes enriched in the inner leaflet of the PL bilayer in a domain of the asymmetric membrane bilayer.
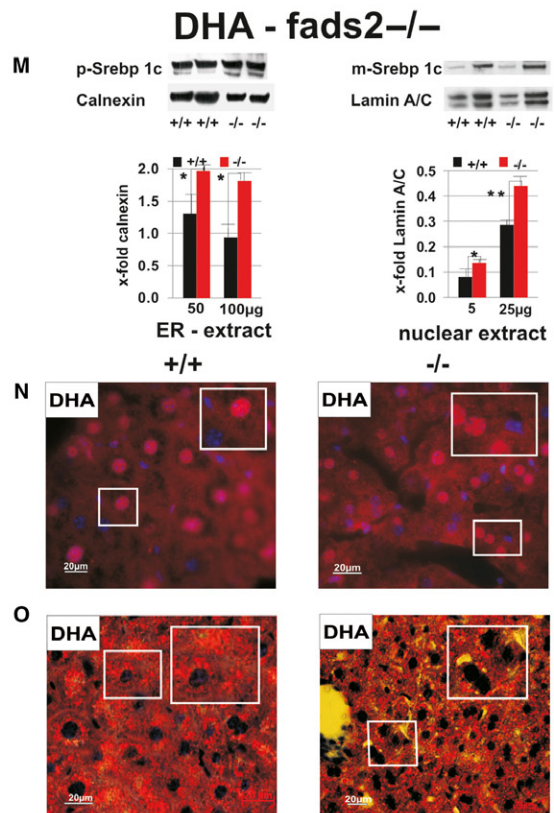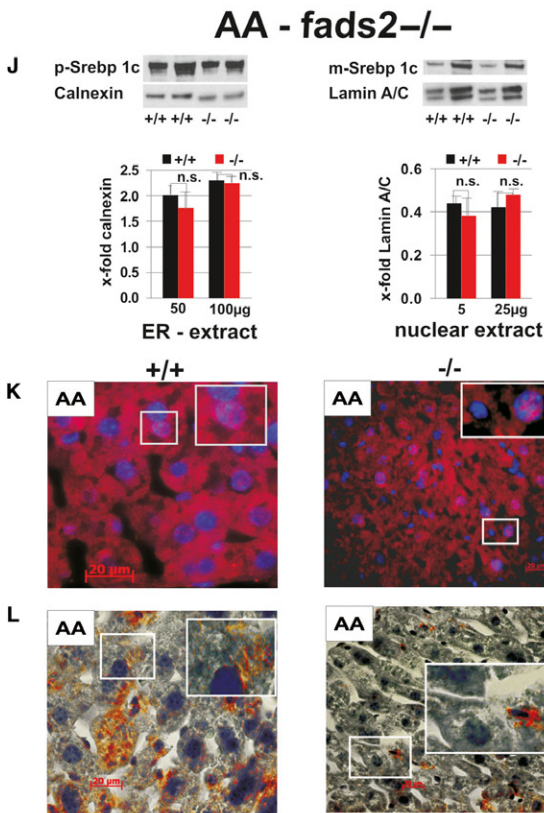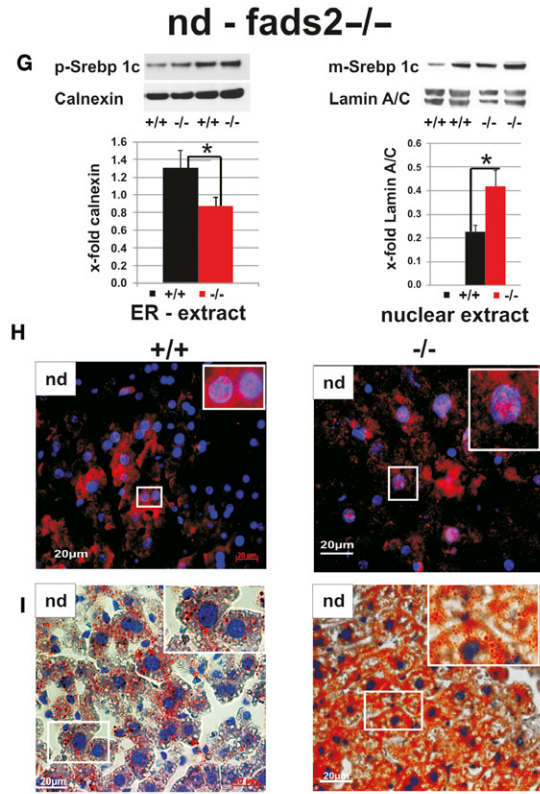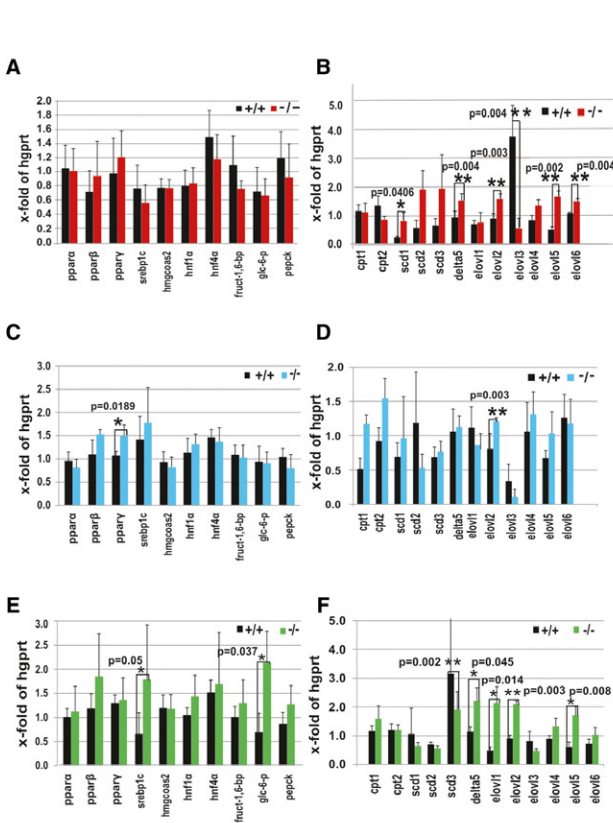
Figure 5. Lipogenesis in the *fads2⁻/⁻* mutant is regulated by the membrane PL environment containing specific PUFA subtituents.

A–F   Expression profiles of genes of transcription factors of enzymes of lipid metabolism, of gluconeogenesis and FA metabolism in liver of *nd-* (A, B), *AA-* (C, D) and *DHA⁺/⁺* and ⁻/⁻ mice (E, F). Elevated gene expression of *scd1*, *Δ5* (*fads1*), *elovl2*, *elovl5* and *elovl6* in liver of *nd⁻/⁻* mice, of *pparγ* and *elovl2* in AA⁻/⁻, and of *sreb1c*, *glc-6-P*, *Δ5* (*fads1*), *elovl1*, *elovl2* and *elovl5* in liver of *DHA⁻/⁻* mice.

G   SREBP1c processing and nuclear import in liver of *nd⁺/⁺* and *nd⁻/⁻* mice. Western blot analysis of ER-proteins of liver of *nd-⁺/⁺* and ⁻/⁻ mice shows a reduced concentration of p-SREBP1c, *P* = 0.042 (C), but enhanced concentration of nuclear m-SREBP1c, *P* = 0.024. *Calnexin* was used as ER- and *lamin A/C* as nuclear protein loading marker.

H   Immuno-histochemistry of *nd⁺/⁺* and ⁻/⁻ cryo-sections of liver were stained with anti SREBP1c antibodies, nuclei with DAPI. Inserts show magnification of nuclei with anti SREBP1c reactive antigen.

I   Oil red-stained cryo-sections (7 μm) of liver from *nd⁺/⁺* showed scarce and from *fads2⁻/⁻* extended lipid droplets (I).

J–O   *AA⁺/⁺* and ⁻/⁻ mice (n = 4) revealed similar concentrations of p-Srebp1c in microsomal (ER) and m-Srebp1c in nuclear protein extract (J), but significantly higher in *DHA⁻/⁻* ER and nuclear extracts (M). In cryosections, nuclei of *AA-fads2⁺/⁺* and ⁻/⁻ hepatocytes were essential-free of SREBP1c antigen as demonstrated by inserts of magnified nuclei (K). Oil red staining indicated that *AA⁺/⁺* and ⁻/⁻ hepatocytes were essentially free of lipid deposits (L), but nuclei of *DHA⁺/⁺* and ⁻/⁻ hepatocytes loaded with SREBP1c antigen (N), massive hepatic steatosis *in DHA⁺/⁺* liver, ameliorated in *DHA⁻/−*mice (O).

transcription factor of enzymes of lipogenesis. Cholesterol concentration in the lipid bilayer of the endoplasmic reticulum and Golgi membranes regulates the membrane-bound steps of processing precursor (p)-SREBP1c to mature (m)-SREBP1c for nuclear import [21].

We therefore studied the impact of the perturbed PL bilayer of microsomal (mic) and of nuclear (nuc) membranes of $nd^{+/+}$ and $^{-/-}$ mice on the posttranslational modification of p-SREBP1c to m-SREBP1c. Western blot analysis of ER- and nuclear membrane lysates using anti-SREBP1c antibodies indicated elevated levels of active m-SREBP1c in the nuclear fraction of $nd^{-/-}$ liver (Fig 5G), which was confirmed by immunohistochemistry (IHC) (Fig 5H). Bright field microscopy of Oil red-stained cryo sections of liver of $nd^{-/-}$ mice revealed hepatocytes filled with tiny lipid droplets (steatosis), compared to few larger diameter droplets in $nd^{+/+}$ hepatocytes (Fig 5I).

Liver of AA-$fads2^{+/+}$ and $AA^{-/-}$ revealed a remarkably similar expression of genes of transcription factors and enzymes of lipogenesis, of except increased expression of *pparγ* and *elovl2* (Fig 5C). Western blot analysis showed a comparable processing of microsomal p-SREBP1c to nuclear m-SREBP1c (Fig 5J), which is supported by IHC indicating a similar nuclear SREBP1c antigen import (Fig 5K). $AA^{-/-}$ hepatocytes were almost free of lipid droplets (Fig 5L).

Only $DHA^{-/-}$ liver RNA showed a threefold higher steady-state concentration of *screbp1c*, of *glc-6p*, a marker of gluconeogenesis, and of *Δ5-desaturase* (*fads1*), elongases *elovl 1, 2* and *5*, which are marker enzymes of PUFA metabolism (Fig 5E and F). Western blot analysis indicated that microsomal p-SREBP1c- and nuclear m-SREBP1c exceeded SREBP1c levels in liver of the $DHA^{+/+}$ mouse (Fig 5M). IHC on liver cryo sections revealed elevated nuclear import of m-SREBP1c and enhanced fluorescent SREBP1c antigen in nuclei of $DHA^{-/-}$ hepatocytes. Nuclei of $DHA^{-/-}$ hepatocytes were heavily loaded with SREBP1c reactive peptides (Fig 5N). Oil red-stained sections of $DHA^{+/+}$ and $^{-/-}$ hepatocytes unveiled hepatic steatosis, characterized by heavy peri-nuclear macro-lipid droplet accumulation. Hepatocytes of $DHA^{+/+}$ and $^{-/-}$ mice differed in number and size of lipid droplets. $DHA^{+/+}$ liver showed heavy steatosis, which was ameliorated in hepatocytes of $DHA^{-/-}$ mice (Fig 5O).

Conclusion

The genetically and biochemically well-defined auxotrophic $fads2^{-/-}$ and the derived AA- and $DHA\ fads2^{-/-}$ mutant mouse lines preclude many of the ambiguities of numerous feeding experiments in rodents in the past, which addressed the important role of PUFAs. This study indicates the wide experimental scope of the auxotrophic $fads2^{-/-}$ mouse. The *nd-*, *AA-* and $DHA^{-/-}$mouse lines might become useful models for unveiling the complex mechanisms underlying the impact of dietary ω3- and ω6-PUFAs in membrane biology, human nutrition and the development and prevention of dyslipidemia, vascular and neurodegenerative diseases due to imbalanced dietary PUFA supply.

Materials and Methods

Reagents

The following antibodies were used for IHC and Western blot analysis: SREBP1c, α-tubulin, lamin A/C, calnexin and affinity-purified polyclonal anti-polypeptide I192-K444 specific rabbit antibodies [9]. DHASCO and ARASCO (Martek Biosciences, Columbia, MD, USA) were used as sources of docosahexaenoic acid (DHA) and arachidonic acid (AA), respectively. [1-¹⁴C] Radioactive and inactive $20:3^{5,11,14}$ were synthesized in this laboratory [9,16,22]. Primers for qRT-PCR are listed under supplementary Table S2.

Animals

Generation and genotyping of $fads2^{+/-}$ and $^{-/-}$ mice have been described before [9]. $Fads2^{+/-}$ mice were back crossed 10 times into the C57BL/6N genetic background. Animals were housed in the SPF-barrier mouse facility of the Center of Molecular Medicine (CMMC) with a 12 h light/dark cycle and free access to water and a regular (*nd*), 20:4-, and 22:6-supplemented (1% of daily caloric uptake) diet (Altromin, Dinslage Germany).The nd-diet was free of PUFAs and optimized with 18:2 and 18:3 to prohibit EFA-deficiency. Colonies of $fads2^{+/+}$, $^{+/-}$, and $^{-/-}$ mice were maintained on the respective diets throughout life time, starting with $fads2^{+/-}$ breeding pairs. FA composition of diets is listed under supplementary Table S1.

Laboratory measurements

Serum concentrations of glucose, insulin, leptin, triglycerides and total cholesterol were determined by standard colorimetric assays [9].

Glucose- and insulin tolerance tests

For GTT and ITT mice were fasted overnight (16 h). Glucose (2 g/kg body weight) was injected intra-peritoneally (ip). For ITT, mice were fasted for 16 h, anesthesized, and insulin (0.5 IU/kg) or saline were injected ip as control. Blood glucose and serum insulin concentrations were determined before and at different times after injection, indicated in the figure legends.

Metabolic measurements

Metabolic parameters (VO_2, VCO_2, H, and RER) were determined in the Phenomaster TSL-system, and fat and lean mass by the Bruker Optics minispec TD-NMRAnalyser. TEWL was measured with the Tewameter, model 210 Courage-Khazaka, Cologne, Germany,

Pulse chase experiments

Primary hepatocyte cultures for pulse chase experiments were prepared from $fads2^{+/+}$ and $^{-/-}$ mice as previously described [23]. Details are provided in Supplementary information.

Gene expression

RNA preparation and real time quantitative RT-PCR (qRT) are described in Supplementary information.

Western blot analysis

Western blot analysis of cell lysates of $fads2^{+/+}$ and $^{-/-}$ liver, muscle, BAT and WAT and nuclear and microsomal proteins of liver is described in Supplementary information.

Immunohistochemistry

Mice were perfused from the left ventricle with PBS and PBS-buffered 4% paraformaldehyde. Organs were fixed and processed for light- and immuno fluorescence microscopy as described in Supplementary information.

Lipid analysis

Isolation, separation, identification and quantification of lipids from organs and subcellular membranes and of fatty acid constituents are described in Supplementary information.

Mass spectroscopy of phospholipids

PL classes were analyzed by MS/MS using an Applied Biosystems (Darmstadt, Germany) QTrap analyzer. Conditions are described in Supplementary information.

Oxidative ozonolysis

FA mixtures of individual PL classes were dissolved in glacial acetic acid/methylacetate 1:2 (v/v) for oxidative ozonolysis. Methylated oxidation products were analyzed by GC/MS as described in Supplementary information.

Statistical analyses

Data are expressed as means ± s.e.m. Differences between two groups were assessed using the unpaired Student's *t*-test. Sizes of animal cohorts are listed under respective figures.

Author contributions

WS designed and performed experiments, BJ, EB IH and ISS performed experiments, SB, MO and MT performed data analysis, WS and IH wrote the manuscript.

Conflict of interest

The authors declare that they have no conflict of interest.

References

1. Crawford MA, Broadhurst CL (2012) The role of docosahexaenoic and the marine food web as determinants of evolution and hominid brain development: the challenge for human sustainability. *Nutr Health* 21: 17–39

2. Calder PC (2006) Polyunsaturated fatty acids and inflammation. *Prostaglandins Leukot Essent Fatty Acids* 75: 197–202

3. Hwang JB, Hernandez J, Leduc R, Frost SC (2000) Alternative glycosylation of the insulin receptor prevents oligomerization and acquisition of insulin-dependent tyrosine kinase activity. *Biochim Biophys Acta* 1499: 74–84

4. Kim KY, Lee JW, Park MS, Jung MH, Jeon GA, Nam MJ (2006) Expression of a thioredoxin-related protein-1 is induced by prostaglandin E(2). *Int J Cancer* 118: 1670–1679

5. Yaqoob P, Calder PC (2003) N-3 polyunsaturated fatty acids and inflammation in the arterial wall. *Eur J Med Res* 8: 337–354

6. Cole GM, Ma QL, Frautschy SA (2009) Omega-3 fatty acids and dementia. *Prostaglandins Leukot Essent Fatty Acids* 81: 213–221

7. Kennedy EP (1961) Biosynthesis of complex lipids. *Fed Proc* 20: 934–940

8. Lands WE, Merkl I (1963) Metabolism of glycerolipids. III. Reactivity of various acyl esters of coenzyme A with alpha'-acylglycerophosphorylcholine, and positional specificities in lecithin synthesis. *J Biol Chem* 238: 898–904

9. Holz B, Jenke B, Binczek E, Günter RH, Kiss C, Karakesisoglou I, Thevis M, Weber AA, Arnhold S, Addicks K (2008) Delta6-desaturase (FADS2) deficiency unveils the role of omega3- and omega6-polyunsaturated fatty acids. *EMBO J* 27: 2281–2292

10. Stroud CK, Nara TY, Roqueta-Rivera M, Radlowski CE, Lawrence P, Zhang Y, Cho BH, Segre M, Brenna JT, Haschek WM, Nakamura MT (2009) Disruption of FADS2 gene in mice impairs male reproduction and causes dermal and intestinal ulceration. *J Lipid Res* 50: 1870–1880

11. Roqueta-Rivera M, Stroud CK, Haschek WM, Akare SJ, Segre M, Brush RS, Agbaga MP, Anderson RE, Hess RA, Nakamura MT (2010) Docosahexaenoic acid supplementation fully restores fertility and spermatogenesis in male delta-6 desaturase-null mice. *J Lipid Res* 51: 360–367

12. Christie WW (1998) Gas chromatography-mass spectrometry methods for structural analysis of fatty acids. *Lipids* 33: 343–353

13. Christie WW, Han X (2010) *Lipid Analysis - Isolation, Separation, Identification and Lipidomic Analysis*, 4th edn. Bridgwater, UK: Oily Press, 446

14. Kangani CO, Kelley DE, Evans RW (2007) Synthesis and mass spectrometry of benzoxazoline, dimethyloxazoline and 4-phenyloxazoline derivatives of polyunsaturated fatty acids. *Rapid Commun Mass Spectrom* 21: 2129−2136

15. Svetashev VI (2011) Mild method for preparation of 4,4-dimethyloxazoline derivatives of polyunsaturated fatty acids for GC-MS. *Lipids* 46: 463−467

16. Nadidai I (1976) Pathway of arachidonic acid. Synthesis of [1-14C] 8,11,14-20:3 and [1-14C]5,11,14 20:3.

17. Matsuda S, Inoue T, Lee HC, Kono N, Tanaka F, Gengyo-Ando K, Mitani S, Arai H (2008) Member of the membrane-bound O-acyltransferase (MBOAT) family encodes a lysophospholipid acyltransferase with broad substrate specificity. *Genes Cells* 13: 879−888

18. Zadravec D, Tvrdik P, Guillou H, Haslam R, Kobayashi T, Napier JA, Capecchi MR, Jacobsson A (2011) ELOVL2 controls the level of n-6 28:5 and 30:5 fatty acids in testis, a prerequisite for male fertility and sperm maturation in mice. *J Lipid Res* 52: 245−255

19. Leonard AE, Kelder B, Bobik EG, Chuang LT, Lewis CJ, Kopchick JJ, Mukerji P, Huang YS (2002) Identification and expression of mammalian long-chain PUFA elongation enzymes. *Lipids* 37: 733−740

20. Westerberg R, Mansson JE, Golozoubova V, Shabalina IG, Backlund EC, Tvrdik P, Retterstol K, Capecchi MR, Jacobsson A (2006) ELOVL3 is an important component for early onset of lipid recruitment in brown adipose tissue. *J Biol Chem* 281: 4958−4968

21. Wang X, Sato R, Brown MS, Hua X, Goldstein JL (1994) SREBP-1, a membrane-bound transcription factor released by sterol-regulated proteolysis. *Cell* 77: 53−62

22. Stoffel W (1961) Biosynthesis of polyenoic fatty acids. *Biochem Biophys Res Commun* 6: 270−273

23. Klingmuller U, Bauer A, Bohl S, Nickel PJ, Breitkopf K, Dooley S, Zellmer S, Kern C, Merfort I, Sparna T, Donaue J, Walz G, Geyer M, Kreutz C, Hermes M, Gotschel F, Hecht A, Walter D, Egger L, Neubert K (2006) Primary mouse hepatocytes for systems biology approaches: a standardized in vitro system for modelling of signal transduction pathways. *Syst Biol* 153: 433−447